Available online at www.sciencedirect.com
SCIENCE DIRECT
Journal of Power Sources 157 (2006) 563–570
JOURNAL OF POWER SOURCES
www.elsevier.com/locate/jpowsour

EIS-in situ characterization of anodic films on antimony and lead–antimony alloys

M. Metikoš-Huković [a,*], R. Babić [a], S. Brinić [b]

[a] *Department of Electrochemistry, Faculty of Chemical Engineering and Technology, University of Zagreb, PO Box 177, 10000 Zagreb, Croatia*
[b] *Faculty of Technology, University of Split, N. Tesle 10, 21000 Split, Croatia*

Received 28 April 2005; received in revised form 27 July 2005; accepted 31 July 2005
Available online 18 October 2005

Abstract

The behaviour of antimony as a function of the concentration of both H_2SO_4 and HSO_4^- ions, and the electrode rotation rate was studied by cyclic voltammetry (CV) and electrochemical impedance spectroscopy (EIS). The rate of antimony dissolution is accelerated with the addition of HSO_4^- ions and with the increasing electrode rotation rate. Impedance measurements of antimony in the region of film formation, and lead and lead–antimony alloys in the region of PbO formation showed that the dissolution rate is controlled by the diffusion through the oxide layer. The diffusion coefficients (D) for protons in the case of antimony dissolution, and for oxygen ions in the case of lead and alloys, were estimated. Electric and dielectric properties of the anodic surface layer of the lead–antimony alloys are significantly influenced by the antimony content.

Keywords: Antimony; Lead–antimony alloys; Lead-acid batteries; Electrochemical impedance

1. Introduction

Antimony is widely used as a constituent of lead alloys for lead/battery grids. Therefore, the electrochemical behaviour of antimony [1–8] and its influence on the electrochemical processes at lead electrode in sulphuric acid solutions [8–17] have been extensively studied. During the anodic polarization of antimony electrode in H_2SO_4 solution, at relatively low overvoltages, a gel-like anodic layer, as a result of primary passivation, is formed [5]. The properties of this layer, which acts as an ionic conductor, were studied using various polarization techniques [1–5,7,8], and impedance spectroscopy [3–8]. Since the anodic dissolution of antimony depends on acid concentration, Pavlov et al. [4] proposed that SO_4^{2-}, and even HSO_4^- may be involved in the mechanism.

It is well known that antimony has a beneficial effect on the performance of lead-acid battery positive plate. Its oxidation in Pb–Sb alloys begins at the potential values at which PbO formation takes place under the $PbSO_4$ perm-selective membrane. It was shown [9,10,13–17] that Sb oxidation in the alloy changes the composition of the anodic layer; simultaneously to the formation of lead oxides, mixed lead and antimony oxides of various compositions, depending on the electrode potential, are formed [9,10].

In the previous papers, we have studied the electrochemical kinetics of anodic layer formation and reduction on antimony and antimonial lead [8]. Mostly we investigated the electrical properties of corrosion layers on the Pb–Sb alloys using EIS method [12,13]. In the present paper, we aimed at EIS examination of the transport processes in surface layers on pure antimony and on Pb–Sb alloys with low antimony content. Also, herein, we investigated the effect of HSO_4^- ions on the anodic dissolution of antimony.

2. Experimental

The study was performed on spectroscopically pure antimony (Johnson Matthey Co.), pure lead (99.998 wt.%) and Pb–Sb alloys with Sb content of 1.3 and 2.7 wt.%. The electrodes had a cylindrical form, and the lateral surface of the cylinder was coated with polyester, exposing only the plane of the cylinder base to the solution; the surface area was 0.46 cm^2. The Sb electrode was polished mechanically, wiped with tissue

* Corresponding author. Tel.: +385 1 4597 140; fax: +385 1 4597 139.
E-mail address: mmetik@marie.fkit.hr (M. Metikoš-Huković).

0378-7753/$ – see front matter © 2005 Elsevier B.V. All rights reserved.
doi:10.1016/j.jpowsour.2005.07.079

Nomenclature

B	fitting parametar
c	molar concentration (mol dm^{-3})
C	capacitance (μF cm^{-2})
d	film thickness (nm)
D_f	diffusion coefficient (cm^2 s^{-1})
E	potential (V)
$\boldsymbol{E}$	electric field strenght (V cm^{-1})
j	current density (mA cm^{-2})
n	fractional exponent
q	charge density (mC cm^{-2})
Q	parameter which contains fractional characteristics of electrochemical system (Ω^{-1} cm^{-2} s^n)
R_d	diffusion resistance (Ω cm^2)
R_Ω	omhic resistance (Ω cm^2)
W	diffusion component
Z_W	impedance of diffusion component (Ω cm^2)

Greek letters

ε	relative dielectric constant
ω	rotation rate (rpm)

paper, dipped in ethanol to remove dust and grease from the surface. Prior to each measurements the electrode was polarized at −300 mV to remove oxides formed on the surface by contact with air. The Pb and Pb–Sb electrodes were polished with SiC paper (600 grit), degreased in ethanol and rinsed with distilled water. Prior to each measurement, the electrodes were polarized at −1.0 V for the same reason mentioned above. Measurements were performed mostly in 0.5 M H_2SO_4 solution. However, electrochemical behaviour of Sb was investigated also in H_2SO_4 solutions of lower and higher concentrations; the solutions were saturated with Sb_2O_3 in order to prevent greater dissolution of antimony.

The experiments were performed in a two-compartment glass cell at 298 K. The counter electrode was a large Pt-plate, and the reference electrode was a saturated calomel electrode (SCE). All potential values are reported in V (mV) versus SCE. Voltammetric measurements were carried out using an EG&G Princeton Applied research Model 273 potentiostat/galvanostat and an EG/G PAR Model 616 rotating disc electrode. The EIS measurements were done using an EG&G M5315A lock-in amplifier in the frequency range from 100 kHz to 30 mHz with the ac voltage amplitude ±5 mV. The impedance spectra were analyzed using the software for complex non-linear last squares (CNLS) fitting developed by Boukamp [18].

3. Results and discussion

3.1. Cyclic voltammetry on pure antimony

Cyclic voltammograms of an antimony electrode, obtained within the potential range from −0.5 to 1.0 V in H_2SO_4 solutions of different concentrations, are presented in Fig. 1. Electrode

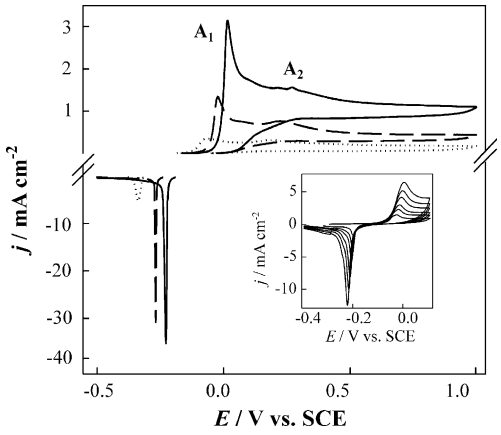

Fig. 1. Cyclic voltammograms on Sb in 0.05 M (····), 0.5 M (- - -) and 5 M (—) H_2SO_4; $\nu = 20$ mV s^{-1}. The inset: cyclic voltammogams recorded in 0.5 M H_2SO_4; $\nu = 10$, 20, 30, 50, 100 and 200 mV s^{-1}.

processes in the anodic and cathodic portions of the Sb voltammetic response have already been discussed in details [3–5,8] and here will be only briefly covered. The anodic portion of the voltammograms starts with a sharp increase in the current density due to the antimony oxidation:

$$Sb + H_2O = SbO^+ + 2H^+ + 3e^- \quad (1)$$

This is a process of active dissolution of antimony. In order to preserve the electroneutrality at the nearby electrode surface, the sulphate ions come from the bulk of the solution, and hydrogen ions leave the surface causing an increase in pH and the formation of a gel-like layer of basic sulphate:

$$SbO^+ + H^+ + SO_4^{2-} = Sb(OH)SO_4 \quad (2)$$

The formation of the $Sb(OH)SO_4$ layer at the electrode surface corresponds to the first current maximum, A_1. With an increase in the acid concentration, partial passivation of the electrode occurs at higher anodic currents, i.e. a higher concentration of SbO^+ ions near the electrode surface is needed for the formation of an anodic layer.

After the formation of the surface layer, the antimony dissolution continues, and when the rate of anodic generation of antimony ions becomes greater than that of the sulphate ions diffusing from the bulk of the electrolyte into the surface layer, the formation of an antimony hydroxide sublayer starts:

$$Sb + 2H_2O = SbOOH + 3H^+ + 3e^- \quad (3)$$

When the entire electrode surface is covered with the SbOOH sublayer, the current maximum A_2 appears at the cyclic voltammogram. With a further potential increase the current decreases slowly showing a current plateau whose height increases with increasing acid concentration. The fairly high currents are accompanied by the high ionic conductivities of the anodic film, and the SbOOH layer grows at about the same rate as it dissolves. This process may be best described by the following reactions:

$$SbOOH + H_2SO_4 = Sb(OH)SO_4 + H_2O \quad (4)$$

$$Sb(OH)SO_4 = SbO^+ + H^+ + SO_4^{2-} \quad (5)$$

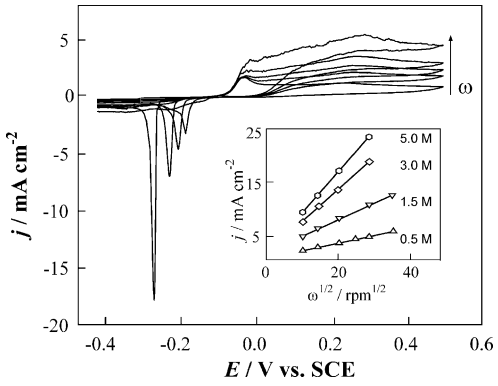

Fig. 2. Cyclic voltammograms Sb in 0.5 M H_2SO_4 as a function of the rotation rate ($\omega = 0$, 100, 400, 800 and 1200 rpm); $\nu = 20\,mV\,s^{-1}$. The inset: the anodic peak A_2 current density as a function of $\omega^{1/2}$ at various concentrations of H_2SO_4.

The thickness of the inner and outer layers is determined by the relation between the rates of reactions (3) and (4) and reactions (4) and (5), respectively.

During the cathodic sweep, a well expressed cathodic peak, whose potential depends upon the acid concentration, is observed. Instead of a single cathodic peak, the two closely overlapping peaks were sometimes observed in this potential range, which is likely due to the experimental conditions.

The inset in Fig. 1 shows the influence of the sweep rate on the CV in the narrow potential range around the rest potential in the 0.5 M H_2SO_4. Analysis of the dependence of the peak current and the peak potential upon the sweep rate showed that the potential-determining reaction occurring at the first anodic and cathodic peak is under the control of ohmic resistance [8].

Fig. 2 shows the effect of the electrode rotation rate on the shape of the CVs obtained in 0.5 M H_2SO_4. With increasing rotation rates, the anodic portions of CVs are shifted to higher currents, and the partial passivation at the peak potential A_1 does not occur ($\omega > 400$ rpm); the first current decrease occurs at the potential of A_2. At all rotation rates used, the cathodic current peak is observed, but with increasing rotation rates its height decreases and position is shifted up to 80 mV toward more positive potential. Bojinov and Pavlov [3] have observed that the cathodic peak potential depends upon the time that the electrode spends at the potential of the A_1 current peak. With an increase in that time (0–15 min), the corresponding cathodic peak was observed at more negative potential values (70–80 mV). They proposed that during a zero electrode stay at A_1 the anodic layer is not formed, and only hydrated antimony ions or complexes undergo reduction. With an increasing time of stay at A_1, the gel formation proceeds, and its reduction occurs at a more negative potential. CVs presented in Fig. 2 show that the same phenomenon occurs here. With increasing rate of electrode rotation, the mass transport of dissolved antimony species becomes higher, and their saturation and film formation is less probable. Consequently, during the cathodic sweep the greater fraction of antimony aqua ions undergo reduction and corresponding cathodic peak moves to positive direction.

Due to the dissolution of the anodic layer, the charge consumption q_a is always greater than q_c. The ratio q_a/q_c at all potentials increases with both increasing rotation rates and acid concentrations.

The inset in Fig. 2 shows the influence of the electrode rotation rate on the anodic current density at A_2 potential for different H_2SO_4 concentrations. Characteristic linear relationship j versus $\omega^{1/2}$ is observed for all acid concentrations.

The Tafel coefficients for the antimony dissolution were determined from the anodic sweeps at the sweep rate of $0.5\,mV\,s^{-1}$. The value of about $42\,mV\,dec^{-1}$ was obtained for 0.05 and 0.5 M H_2SO_4, and that of about $23\,mV\,dec^{-1}$ for 5 M H_2SO_4. The obtained values correlate well with those given in literature. Pavlov at al. [4] found the slope of 25 mV for the dissolution of Sb in 4.5 M H_2SO_4, and 41 mV in 0.5 M H_2SO_4. The Tafel slopes obtained could be correlated with the following mechanism of antimony dissolution in H_2SO_4 [7]:

$$Sb + H_2O = SbOH_{ad} + H^+ + e^- \quad (6)$$

$$SbOH_{ad} = SbO_{ad} + H^+ + e^- \quad (7)$$

$$SbO_{ad} = SbO^+ + e^- \quad (8)$$

Since corrosion rates of Sb, at open circuit potential, increase linearly with acid concentration, Pavlov et al. [4] concluded that sulphate or hydrogensulphate can participate in the anodic dissolution of antimony, and accordingly modified the above mechanism by adding the following step:

$$SbO_{ad} + HSO_4^- = Sb(OH)SO_4 + e^- \quad (9)$$

According to the above mechanism, if the reaction (7) is rate-limiting, the reaction (6) in equilibrium, and the steps (8) and (9) are fast, the Tafel slope is 39 mV. This situation corresponds to the Sb dissolution in 0.05 and 0.5 M H_2SO_4. On the other hand, if the reaction (9) is the rate determining step, then the Tafel slope is 25 mV; such is the case with higher acid concentrations.

To test the influence of HSO_4^- ions on the corrosion rate of Sb in H_2SO_4, we performed the quasi-potentiostatic measurements with different concentrations of $NaHSO_4$ in 0.5 M H_2SO_4 at a constant pH in the Tafel region. The results obtained clearly show that the intersection of cathodic and anodic slopes shifted towards the higher current densities with increasing HSO_4^- concentration, i.e. that the HSO_4^- ions accelerate the corrosion of Sb in H_2SO_4. An increase in concentration of HSO_4^- ions did not influence the anodic Tafel slope. These results support the modified mechanism of Sb dissolution in H_2SO_4.

3.2. Impedance measurements on pure antimony

Impedance measurements were performed with a stationary and rotating Sb electrode in 0.5 M H_2SO_4 in the potential ranging from −0.11 to 1.5 V. Measurements were also performed in 0.5 M H_2SO_4 with addition of HSO_4^- ions, and only with a stationary Sb electrode.

3.2.1. Impedance measurements on the stationary electrode

Impedance spectra obtained with a stationary Sb electrode in 0.5 M H_2SO_4 are selected according to the equivalent circuits used to analyse the data.

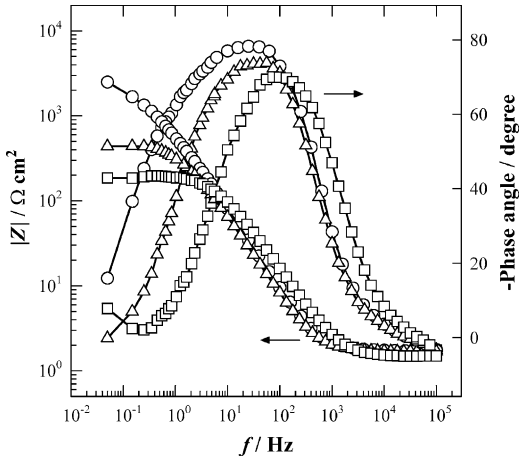

Fig. 3. Bode plots for Sb at −0.11 V (◯), −0.08 V (△) and −0.05 V (□) in 0.5 M H_2SO_4.

The impedance spectra obtained in the potential range of active antimony dissolution (at potentials less negative than $E(A_1)$) are presented in Fig. 3 in the form of Bode plots. The spectra show that in the higher frequency region, log $|Z|$ tends to become constant with the phase angle values falling rapidly towards 0° with increasing frequency. This is a response typical of resistive behaviour and corresponds to the solution resistance. In the medium frequency region, a linear relationship between log $|Z|$ and log f is observed with a slope close to −1, and a phase angle approaching −90°. In the low-frequency range, the resistive behaviour of the electrode becomes more pronounced, but the region where log $|Z|$ does not depend on log f (i.e. the dc limit) is not reached until 10^{-2} Hz. These Bode plots have the elements characteristic of a R_p–C parallel combination in series with an ohmic resistance (Fig. 4a). Since the slope of log $|Z|$ versus log f plot is not −1 and the phase angle does not amount to −90°, the electrode impedance may be precisely described by a constant-phase element (CPE): $Z(\mathrm{CPE}) = [Q(j\omega)^n]^{-1}$, where Q is the constant, ω the angular frequency, and n is the CPE power. The n is an adjustable parameter that usually lies between 0.5 and 1 [19], the ideal capacitor is described with $n = 1$. Table 1 shows numerical values for the circuit parameters. The R_Ω being $1.7 \pm 0.1\ \Omega\,\mathrm{cm}^2$ was observed in the whole potential region. Since the n values are close to 1, Q represents the double layer capacity that is parallel to the charge transfer resistance, R_p. With an increase in anodic polarization the R_p decreases showing the rise in anodic dissolution of antimony in accordance with the CV presented in Fig. 1.

The impedance spectra obtained when the potential is above 0.2 V, where the Sb electrode is partially passivated, are given in

Table 1
The EEC parameters for Sb at selected potentials in the active region in 0.5 H_2SO_4

E (V)	Q ($\times 10^6\ \Omega^{-1}\,\mathrm{cm}^{-2}\,\mathrm{s}^n$)	n	R ($\times 10^{-2}\ \Omega\,\mathrm{cm}^2$)
−0.11	314	0.90	22.20
−0.08	359	0.95	4.29
−0.05	205	0.89	1.96

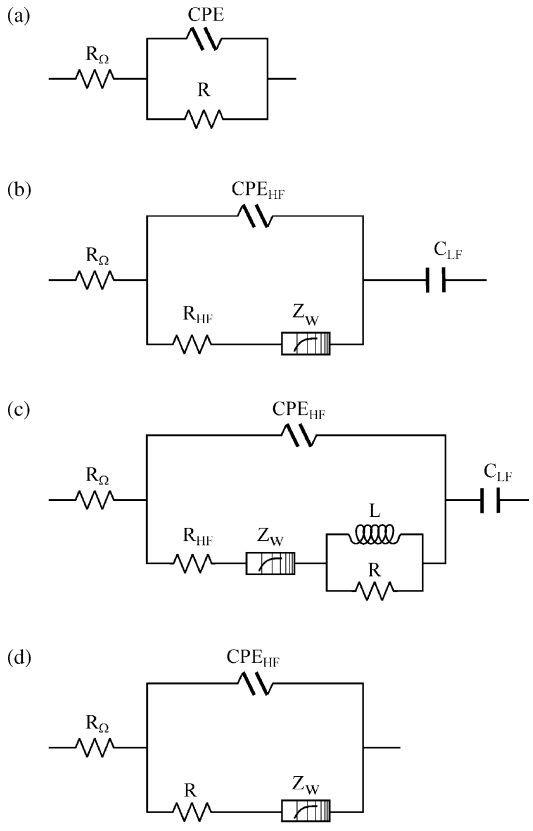

Fig. 4. Equivalent circuits used to fit experimental data.

Fig. 5 in the form of Bode plots. The plot suggests the presence of at least two time constants. The high frequency time constant may be related to the charge transfer process at the film/solution interface, while the other time constant is related to the intermediate steps of anodic antimony dissolution and surface film formation, detected at intermediate and low frequencies. The electrical equivalent circuit given in Fig. 4b represents the best fit of experimental data. The total impedance, Z, of the electrochemical system was found by adding the resistance of the electrolyte, R_Ω to the impedance of the electrochemical inter-

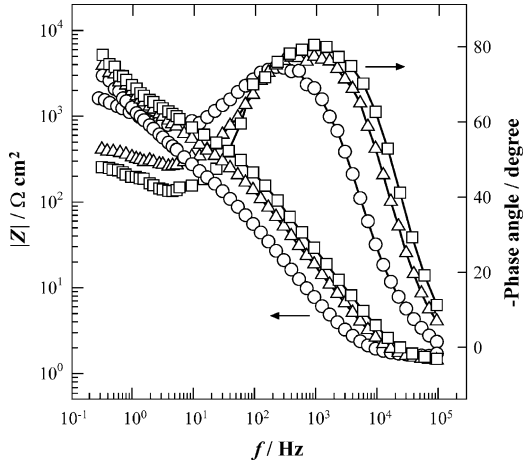

Fig. 5. Bode plots for Sb at 0.4 V (◯), 1.0 V (□) and 1.5 V (△) in 0.5 M H_2SO_4.

face:

$$Z = R_\Omega + \frac{1}{Q(j\omega)^n + [R_{HF} + Z_W]^{-1}} + (j\omega C_{LF})^{-1} \quad (10)$$

where R_{HF} is the high frequency resistance, and C_{LF} is the low frequency capacitance. The term W represents dimensional diffusion through a layer of finite thickness, whose impedance is given by [20,21]:

$$Z_W = \frac{R_d \tanh[B\sqrt{j\omega}]}{B\sqrt{j\omega}} \quad (11)$$

where R_d is the diffusion resistance, and B is the fitting parameter. The diffusion through a layer of finite thickness, whose impedance can be given by the Eq. (11) or by the cot h function [21] was often discussed in the systems: metal/surface oxide layer/electrolite solution [22–25].

The impedance parameters obtained by fitting experimental to the theoretical values of the EEC are presented in Table 2. The R_Ω being $1.6 \pm 0.2\ \Omega\,cm^2$ was observed in the whole potential region. The dependence of the reciprocal value of the capacitance C_{HF} on the potential >0.2 V is linear. This relationship confirms the identification of the capacitance with the one of the growing film. In this case, we can express dC_{HF}/dE as

$$\frac{dC_{HF}}{dE} = (\varepsilon\varepsilon_0 \boldsymbol{E})^{-1} \quad (12)$$

Using the value for the field strength obtained from our galvanostatic experiments [26], $\boldsymbol{E} = 2.7 \times 10^6\ V\,cm^{-1}$, the dielectric constant of the film can be calculated, $\varepsilon = 32$. It is hard to compare the so obtained value with the one for bulk crystalline Sb_2O_3 ($\varepsilon = 12.8$), due to the higher disorder and hydration of anodic films.

Since the Warburg impedance was assessed as being a film diffusion process where the diffusion layer thickness, d, can replace the thickness of the film through which the diffusion takes place [27], it follows that the parameter $B = d(1/D_f)^{1/2}$, where D_f is the film diffusion coefficient. The film thickness ($d = 48$ nm) was calculated from the cathodic charge ($49\ mC\,cm^{-2}$) consumed during reduction of the anodic layer formed at the potential of 1.0 V during a period of 10 min (the time needed to reach a steady state conditions) under assumption that the film composition corresponded to Sb_2O_3. For $B = 1.11\ s^{0.5}$ (Table 2), a $D_f = 1.9 \times 10^{-11}\ cm^2\,s^{-1}$ is obtained, which is in a good agreement with D_f usually reported for diffusion of protons in solid films. Bojinov and Pavlov [3] determined the D_f for the protons to be of the order of $10^{-11}\ cm^2\,s^{-1}$ for antimony layer in 0.5 M H_2SO_4 at a potential close to the anodic maximum A_2. For the oxide film on ruthenized gold, Metikoš-Huković et al. [28] calculated an effective diffusion coefficient of protons to be between 10^{-10} and $10^{-11}\ cm^2\,s^{-1}$.

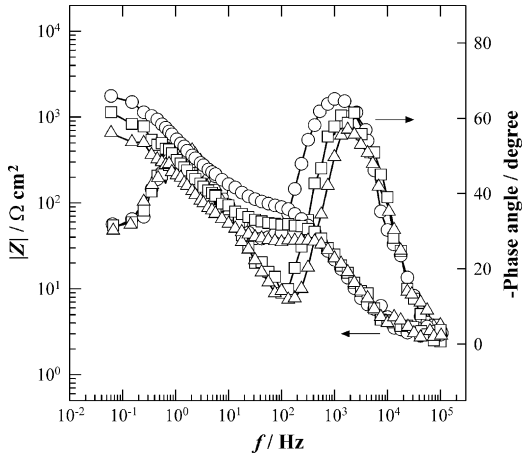

Fig. 6. Bode plots for Sb at 1.0 V as a function of rotation rate in 0.5 M H_2SO_4 $\omega = 100$ rpm (◯), 400 rpm (□) and 1200 rpm (△).

3.2.2. Impedance measurements on the rotating Sb electrode

Impedance measurements with a rotating antimony electrode in 0.5 M H_2SO_4 were performed at the same potentials as those with a stationary one. The spectra obtained at 1.0 V at different rotation rates of the electrode are presented in Fig. 6, while the EEC used to fit the experimental data is shown in Fig. 4c. In addition to the EEC used for a stationary Sb electrode, an inductance, of magnitude L, in parallel with R, had to be introduced to data fitting. Generally, the origin of the inductance can be influenced by some adsorbed intermediates or can be a result of a space charge at the interfaces. The origin of the inductance in the frequency range between 50 and 500 Hz can be related to a rearrangement of surface charge (space charge) at the metal/oxide interface. This charge influences the transport of mobile charge carriers across the anodic film [29–32].

The impedance parameters obtained by fitting experimental to the theoretical values of the EEC are given in Table 3. The R_Ω changed from 2.9 to 3.8 $\Omega\,cm^2$ with increasing rotation rate from 100 to 1200 rpm. Significantly lower R_{HF} and R_d values

Table 2
The EEC parameters for Sb at selected potentials in the passive region in 0.5 H_2SO_4

E (V)	Q_{HF} ($\times 10^6\ \Omega^{-1}\,cm^{-2}\,s^n$)	n	R_{HF} ($\Omega\,cm^2$)	B ($s^{0.5}$)	R_d ($10^{-3}\ \Omega\,cm^2$)	C_{LF} ($\times 10^{-3}\ \mu F\,cm^{-2}$)
0.20	108.2	0.87	251	4.23	1.19	–
0.25	78.7	0.89	281	2.40	2.40	–
0.30	63.8	0.89	288	1.29	2.12	–
0.40	36.8	0.92	169	0.94	3.13	0.22
0.60	23.3	0.92	307	0.61	2.54	0.26
0.80	16.1	0.93	356	1.00	3.70	0.10
1.00	11.1	0.95	408	1.11	6.53	0.44
1.50	6.9	0.96	502	1.07	5.63	0.36

Table 3
The EEC parameters for Sb at 1.0 V as a function of the rotation rate in 0.5 H_2SO_4

ω (rpm)	Q_{HF} ($\mu F\,cm^{-2}$)	n	R_{HF} ($\Omega\,cm^2$)	B ($s^{0.5}$)	R_d ($\Omega\,cm^2$)	R ($\Omega\,cm^2$)	L (He cm^{-2})	C_{LF} ($\times10^{-3}$ $\mu F\,cm^{-2}$)
100	11.1	0.95	47.3	0.87	935	41	0.10	1.44
400	7.6	0.98	27.2	0.78	443	27	0.04	1.95
1200	6.9	0.99	19.0	0.66	204	16	0.02	1.95

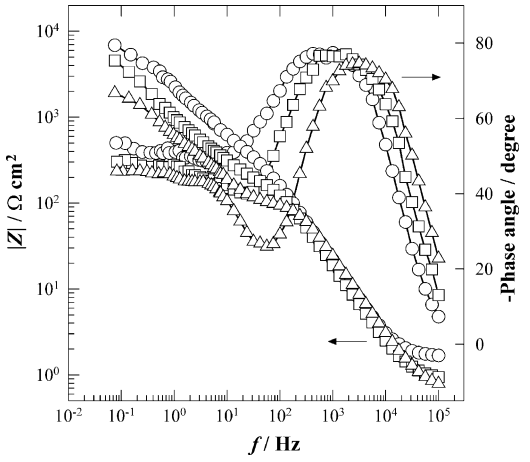

Fig. 7. Bode plots for Sb at 1.0 V as a function of concentration of HSO_4^- ions in 0.5 M H_2SO_4; $c(HSO_4^-)$ = 0.5 M (◯), 0.9 M (□) and 1.7 M (△).

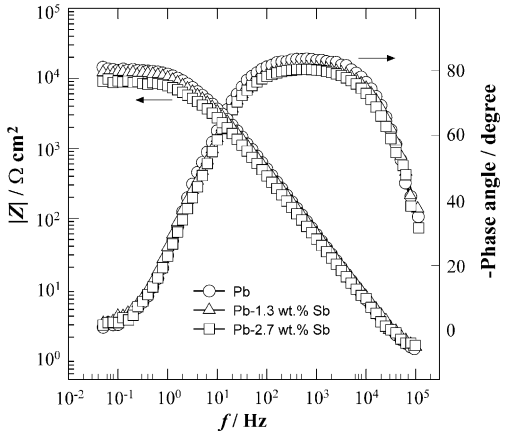

Fig. 8. Bode plots for Pb and Pb–Sb at 0.2 V in 0.5 M H_2SO_4.

were seen when impedance parameters are compared with those for a stationary electrode at the same potential.

For a rotating electrode, the dependence of the reciprocal value of the capacitance C_{HF} upon potential above 0.2 V is also linear, confirming the identification of the capacitance with that of the growing film. Table 3 shows that the parameter B decreases with increasing rotation rate. Since the thickness of the layer also decreases with increasing rotation rate (31.2 nm at 100 rpm), the D_f (calculated from the parameter B) of the order of 10^{-11} $cm^2\,s^{-1}$ can be considered independent upon the rotation rate.

3.2.3. Influence of HSO_4^- ions on anodic behaviour of Sb

Impedance measurements with a stationary antimony electrode in 0.5 M H_2SO_4 containing different levels of hydrogensulphate were performed at the same potentials as those in a pure acid. As an example, the spectra obtained at 1.0 V are shown in Fig. 7. Spectra got in a solution with a lower HSO_4^- concentration were fitted with the EEC presented in Fig. 4b, while for the spectra collected at a higher concentration of HSO_4^- the EEC with an inductance element (Fig. 4c) was used. Numerical values of impedance parameter obtained by the fitting procedure are given in Table 4. With increasing concentration of HSO_4^-, the R_Ω decreased from 1.7 to 0.7 $\Omega\,cm^2$. The results obtained show that the increasing concentration of HSO_4^- ions influences mostly the R_{HF} and C_{LF}, i.e. the influence of HSO_4^- ions is similar to that of electrode rotation rate. This observation is consistent with potentiodynamic measurements which showed that HSO_4^- ions accelerate the anodic dissolution of antimony, and justify their role, proposed by Pavlov et al. [4], in the mechanism of anodic dissolution of antimony in sulphuric acid solution.

3.3. Impedance measurements on antimonial lead

In order to study the influence of antimony on the electrochemical behaviour of lead in the potential range of lead oxide, electrochemical impedance measurements were performed on two low-antimony alloys: Pb–1.3 wt.% Sb and Pb–2.7 wt.% Sb. A parallel investigation was also performed on a pure Pb electrode, on which a duplex passive layer composed of tet-PbO and $PbSO_4$ is formed in the examined potential range. Fig. 8 shows the spectra in the form of Bode plot for pure-Pb and Pb–Sb alloys obtained after they had been oxidized at 0.2 V for 60 min. The EEC which has given the best fit of the experimental data is presented in Fig. 4d, while the values for the equivalent circuit elements are listed in Table 5. The value of R_Ω equal to 1.0 $\Omega\,cm^2$ for all electrodes represents the electrolyte resistance of sulphuric acid. Since n values are close to 1, Q_{HF} corresponds to a

Table 4
The EEC parameters for Sb at 1.0 V in 0.5 M H_2SO_4 with addition of HSO_4^- ions

c (HSO_4^-) (M)	Q_{HF} ($\mu F\,cm^{-2}$)	n	R_{HF} ($\Omega\,cm^{-2}$)	B ($s^{0.5}$)	R_d ($\times10^{-3}$ $\Omega\,cm^{-2}$)	R ($\Omega\,cm^{-2}$)	L (He cm^2)	C_{LF} ($\times10^{-3}$ $\mu F\,cm^{-2}$)
0.5	11.1	0.95	408	1.11	6.53	–	–	0.44
0.9	12.2	0.95	134	1.00	2.08	–	–	1.00
1.7	9.5	0.95	37	1.31	1.87	56	0.13	6.00

Table 5
The EEC parameters for Pb and Pb–Sb at 0.2 V in 0.5 M H_2SO_4

Sb (wt.%)	Q ($\mu F\,cm^{-2}$)	n	R ($\times 10^{-3}\,\Omega\,cm^2$)	B ($s^{0.5}$)	R_d ($\times 10^{-3}\,\Omega\,cm^2$)
0.0	4.55	0.94	7.47	0.37	5.73
1.3	5.53	0.91	7.25	0.45	5.26
2.7	7.04	0.91	6.20	0.44	4.77

capacitor, and, thus, C_{HF} and R_{HF} are associated with the capacitance and resistance of the passive layer, respectively. Since the porosity of outer $PbSO_4$ layer in 0.5 M H_2SO_4 is high [33] in comparison to that formed in acid of much higher concentration [34], its electrical contribution to the passive layer can be neglected for this acid concentration and C_{HF} and R_{HF} can be treated as the capacitance and resistance of the inner PbO barrier layer. Pavlov [35] proposed a solid-state mechanism for the growth of the PbO layer, and the rate of oxidation of Pb to tet-PbO is governed by the solid-state diffusion of interstitial O^{2-} anions through the PbO layer [35,36] by a vacancy mechanism. Thus, the diffusion resistance, R_d of the oxide layer is equal to [21]:

$$R_d = \left(\frac{RT}{z^2F^2}\right)\left(\frac{d}{D_f c}\right) \quad (13)$$

where c is the concentration of O^{2-} ions at the electrolyte/oxide boundary, z and D are the charge and diffusion coefficient of O^{2-} ions, respectively, and d is the thickness of the oxide layer. Both R_d and the parameter B (d^2/D_f) are presented in Table 5. The results in Table 5 show that the electrical properties of a barrier PbO layer, which is responsible for passivation of low antimony alloys in 0.5 M H_2SO_4 are dependent upon the Sb content. The R_{HF} of the oxide film decreases with increasing antimony content. In the same way, the R_d, the diffusion resistance of O^{2-} ions, depends upon the Sb content. Rocca and Steinmetz [17] have shown that the oxide thickness increases almost linearly during the time of 20 h of potentiostatic polarization, and that the obtained thickness does not change very much for alloys with the Sb-content between 1.3 and 3 wt.%. Taking into account their findings, it was possible to estimate the oxide layer thickness to be of the order of 10^{-6} cm, and accordingly the diffusion coefficient of O^{2-} ions to be in the range of 10^{-12} to $10^{-13}\,cm^2\,s^{-1}$. The obtained values, although smaller than those found by Rocca et al. [17] for much thicker oxide layers, seem quite reasonable.

It was established that antimony in Pb–Sb alloys is oxidized at potentials higher than −0.40 V (versus Hg/Hg_2SO_4), i.e. in the PbO potential region. Sb is dissolved in the form of SbO^+ ions, part of which remains in the PbO layer being incorporated into the crystal lattice of the PbO oxide. According to Pavlov et al. [10], in the lead oxide potential range some of Pb^{2+} ions are replaced by Sb^{3+} ions, whereby the crystal lattice of the PbO is preserved unchanged. These substituted oxides have a variable non-stoichiometric composition. At potentials up to 0.8 V (versus Hg_2SO_4), the oxide layer is of a mosaic-like structure composed of both tet-PbO and mixed oxide, that can be presented as $Pb_{(1-x)}Sb_xO$. The impedance results show that Sb ions incorporated into the PbO structure increase conductivity of the oxide layer.

4. Conclusions

Anodic dissolution of antimony as a function of sulphuric acid and HSO_4^- concentrations, and the rotation rate of the electrode was studied by CV, quasi-potentiostatic and EIS methods. The EIS method was also used to investigate the anodic behaviour of Pb–Sb alloys with Sb content of 1.3–3.5% in the potential range of PbO formation.

The results of all applied methods showed that the rate of anodic dissolution of antimony increases with increasing concentration of H_2SO_4. It is also accelerated by the addition of HSO_4^- ions and with increasing rotation rate of the Sb-electrode. The results of EIS measurements showed that anodic dissolution of antimony in the potential range of oxide formation is controlled by diffusion through the oxide layer. The finite diffusion impedance is analysed using a diffusion factor (B). The layer thickness (d) is determined from the cathodic charge assuming Sb_2O_3 as the oxide layer, and the diffusion coefficient (D_f) corresponding to the diffusion of protons, which was estimated to be $D_f(H^+) = 4 \times 10^{-12}\,cm^2\,s^{-1}$. It was found that $D_f(H^+)$ does not depend on the rotation rate of the electrode.

The EIS data show that the PbO growth is controlled by the diffusion of O^{2-} species through the oxide layer; its diffusion coefficient was estimated to be in the range of 10^{-12} to $10^{-13}\,cm^2\,s^{-1}$. The results show that Sb ions incorporated within the PbO structure increase the conductivity of the oxide layer.

References

[1] Metikos-Hukovic, B. Lovrecek, Electrochim. Acta 25 (1980) 717.
[2] Metikos-Hukovic, B. Lovrecek, Electrochim. Acta 23 (1978) 137.
[3] M. Bojinov, D. Pavlov, J. Electroanal. Chem. 315 (1991) 201.
[4] D. Pavlov, M. Bojinov, T. Laitinen, G. Sundholm, Electrochim. Acta 36 (1991) 2081.
[5] D. Pavlov, M. Bojinov, T. Laitinen, G. Sundholm, Electrohim. Acta 36 (1991) 2087.
[6] M. Bojinov, I. Kanazirski, A. Girginov, Electrochim. Acta 41 (1996) 2695.
[7] S. Laihonen, T. Laitinen, G. Sundholm, A. Yli-Pentti, Electrochim. Acta 35 (1990) 229.
[8] M. Metikos-Hukovic, R. Babic, S. Omanovic, J. Electroanal. Chem. 374 (1994) 199.
[9] B. Monahov, D. Pavlov, J. Electrochem. Soc. 141 (1994) 2316.
[10] D. Pavlov, B. Monahov, G. Sundholm, T. Laitinen, J. Electroanal. Chem. 305 (1991) 57.
[11] D. Pavlov, B. Monahov, J. Electroanal. Chem. 218 (1987) 135.

[12] M. Metikos-Hukovic, R. Babic, S. Brinic, J. Power Sources 64 (1997) 13.
[13] S. Brinic, M. Metikos-Hukovic, R. Babic, J. Power Sources 55 (1995) 19.
[14] R. Babic, M. Metikos-Hukovic, N. Lajqy, S. Brinic, J. Power Sources 52 (1994) 17.
[15] Q. Sun, Y. Guo, J. Electroanal. Chem. 493 (2000) 123.
[16] Y. Guo, J. Yue, C. Liu, Electrochim. Acta 38 (1993) 1131.
[17] E. Rocca, J. Steinmetz, J. Electoanal. Chem. 543 (2003) 153.
[18] A. Boukamp, Solid-State Ionic 20 (1986) 31.
[19] U. Rammelt, G. Reinhard, Electrochim. Acta 35 (1990) 1045.
[20] I. Epelboin, M. Keddam, J. Electrochem. Soc. 117 (1970) 1052.
[21] J.R. Macdonald, Impedance spectroscopy, in: Emphasising Solid Materials and Systems, Wiley, New York, 1987, p. 88.
[22] R. Babić, M. Metikoš-Huković, Thin Solid Films 359 (2000) 88.
[23] M. Metikoš-Huković, R. Babić, A. Marinović, J. Electrochem. Soc. 145 (1998) 4045.
[24] M.M. Ficquelmomt-Loizos, H. Takenouti, W. Kante, J. Electroanal. Chem. 428 (1997) 129.
[25] L.M. Gassa, H.T. Mishima, B.A.L. Mishima, J.R. Vilche, Electrochim. Acta 42 (1997) 1717.
[26] S. Brinic, M. Metikos-Hukovic, R. Babic, EUROCORR′96, Nice 1996, Extended Abstracts, X-P13, 1–5.
[27] R.P. Buck, J. Electroanal. Chem. 18 (1977), 363, 381 and 387.
[28] M. Metikoš-Huković, R. Babić, F. Jović, Z. Grubač, Electrochim. Acta 50 (2005) in press.
[29] M. Metikoš-Huković, Z. Grubač, J. Electroanal. Chem. 556 (2003) 167.
[30] D.D. Macdonals, S.R. Biaggio, H. Song, J. Electrochem. Soc. 139 (1992) 170.
[31] J.H.W. de Wit, H.J.W. Lenderink, Electrochim. Acta 41 (1996) 1111.
[32] J. Bessone, C. Mayer, K. Juttner, W. Lorenz, Electrochim. Acta 28 (1983) 171.
[33] N. Stein, E. Rocca, R. Kleim, J.M. Lecuire, T. McRae, Electrochim. Acta 44 (1998) 445.
[34] F.E. Varela, L.M. Gassa, J.R. Vilche, J. Electoanal. Chem. 353 (1993) 147.
[35] D. Pavlov, Electrochim. Acta 23 (1978) 845.
[36] E. Rocca, J. Steinmetz, S. Weber, J. Electochem. Soc. 146 (1999) 54.